A Numerical Experiment on the Breakdown of a Polar Vortex due to Forced Rossby Waves

By Shigeo Yoden and Keiichi Ishioka

Department of Geophysics, Kyoto University, Kyoto 606-01, Japan
(Manuscript received 26 August 1992, in revised form 18 November 1992)

Abstract

In order to get a deeper insight into the stratospheric circulation during sudden warming events, evolution of a circumpolar vortex perturbed by forced Rossby waves is investigated for a wide range of external parameters by using a high-resolution barotropic model in a spherical domain.

If the amplitude of the wave forcing is large, the main polar vortex breaks down and the absolute vorticity is mixed irreversibly over the hemisphere. On the other hand, the main vortex migrates off the pole during the forcing period but returns to the pole afterwards without much erosion, if the amplitude of the forcing is small. The evolution of the polar vortex depends not only on the amplitude of wave forcing but also on other parameters such as latitudinal and longitudinal scales of the forcing, intensity of the polar vortex and latitudinal configuration of the vortex. The polar vortex breaks easily, if latitudinal extent of the forcing is wide or zonal wavenumber of the forcing is not 1 but 2. If the initial polar vortex is strong enough, there is a clear separation between the two types of the response at a critical amplitude of the wave forcing, *i.e.*, breakdown or migration of the main polar vortex. Moreover, the evolution is highly dependent on the latitudinal configuration of the initial zonal wind over the globe: If the initial zonal wind is symmetric with respect to the equator, the vortex breaks easily. On the other hand, it is very robust if the zonal wind is anti-symmetric.

1. Introduction

McIntyre and Palmer (1983, 1984) introduced a new paradigm of breaking planetary waves and erosion of the circumpolar vortex in the winter stratosphere using daily maps of Ertel's potential vorticity (PV) on the 850 K isentropic surface. The PV map is a powerful tool to diagnose the wintertime stratospheric circulation, including stratospheric sudden warming events. Observational support for the paradigm has been provided with several kinds of data and analyses. Leovy, *et al.* (1985) used the Nimbus 7 LIMS data for diagnosis of ozone variations in the middle stratosphere to show the evidence for planetary wave breaking. Using the same LIMS data, Butchart and Remsberg (1986) computed the area index of the polar vortex, an objective definition of which had been given by McIntyre and Palmer (1984), to diagnose evolution of the stratospheric circulation and tracer transport on an isentropic surface. Year to year variations of the polar vortex and planetary wave breaking were investigated by Clough, *et al.* (1985) with the PV diagnosis using the Tiros-N SSU data for five years, and by Baldwin and Holton (1988) using the NMC data for the years 1964–82.

Some minor constituents in the stratosphere, such as ozone, water vapor and nitric acid, were used in some of these diagnostic studies to show the tracer transport during wave breaking events. The constituents are irreversibly mixed outside the main polar vortex, while those in the vortex are isolated from the mid-latitude air. It has been widely recognized that the isolation of polar air in wintertime has an important dynamical effect on the process of the Antarctic ozone depletions (McIntyre, 1989; Schoeberl and Hartmann, 1991).

A numerical experiment on the breaking planetary waves was done by Juckes and McIntyre (1987, hereafter referred to as JM) with a high-resolution one-layer hemispheric model. A prescribed zonally-symmetric polar vortex similar to the real winter stratosphere was perturbed by a time-dependent, quasi-topographic wave forcing of zonal wavenumber 1. They obtained a clear evidence of breaking planetary waves and isolation of fluid inside the vortex from the surroundings. Motions in small scales, such as small vortices and thin filaments in the PV fields, are significant in the breaking process, which is indicative of the importance of nonlinear interactions within a wide spectrum of horizontal scales. The isolation of the main polar vortex is well recognized by sharp gradients of PV at the edge of the vortex. The sharpness of the gradients raises a question on the eddy-diffusive hypothesis for large-scale motions in the stratosphere (McIntyre, 1990). Further experiments on the dynamics of the polar vortex have been done with several kinds of two-dimensional models (Juckes, 1989; Salby, *et al.*, 1990a, b, c; O'Sullivan and Salby, 1990; Polvani and Plumb 1992). Haynes (1990) did a similar experiment with a high-resolution three-dimensional model and pointed out that two-dimensional vortex dynamics can provide considerable insight into the behavior of three-dimensional stratified and rapidly rotating flow.

Kouker and Brasseur (1986) made a numerical study on the tracer transport during a stratospheric sudden warming event with a simple three-dimensional model. Their result shows intrusion of a small, well-organized tongue of subtropical air into the polar cap and strong quasi-horizontal mixing in mid-latitude "surf zone", even though the spatial resolution of their model is not very high. Similar numerical simulations of a stratospheric sudden warming event were done by Mahlman and Umscheid (1987) and O'Neill and Pope (1988) with different numerical models; similar patterns of planetary wave breaking to those observed in satellite data were obtained in diagnoses of a passive tracer and PV in their numerical results.

Most of these numerical studies were limited to some particular cases close to the real stratosphere, because their main subjects were to investigate the evolution of the flow field in detail, such as transport properties of the realized flow, formation of sharp PV gradients at the edge of the vortex, and so on. Details on the sensitivity of the evolution to experimental parameters have not been reported yet except for the work by Polvani and Plumb (1992). They made a "methodical sweep of parameter space" using the method of Contour Dynamics/Contour Surgery to get a deeper understanding of the complex non-linear dynamics of an isolated vortex perturbed by forced Rossby waves.

In this study, eleven series of numerical experiments with a high-resolution barotropic spherical model are done for a wide range of external parameters. The sensitivity of the evolution to the parameters, such as amplitude of the wave forcing, latitudinal and longitudinal scales of the forcing, intensity of the polar vortex and latitudinal configuration of the vortex, is investigated. As a primitive measure of the flow field, the mean zonal wind at a given latitude is used to diagnose the evolution of the polar vortex, as well as daily PV maps. In addition to the breakdown of the polar vortex, its recovery process is also investigated to understand the relative importance of the diabatic process to the dynamic one. Model and experimental procedure are described in Section 2, and results are given in Section 3. Discussion is made in Section 4, and conclusions are in Section 5.

2. Model and experimental procedure

We use a non-divergent barotropic vorticity equation similar to that introduced by JM:

$$DQ/Dt = (\nu\Delta^3 - \alpha)(Q - Q_0), \tag{1}$$

where t is time and D/Dt the material derivative. The dependent variable Q is defined as

$$Q(\lambda, \phi, t) = \zeta_a(\lambda, \phi, t) + F(\lambda, \phi, t), \tag{2}$$

where ζ_a is the absolute vorticity and F is a prescribed, quasi-topographic forcing function. Spherical coordinates (λ, ϕ) are longitude and latitude, respectively. Two kinds of damping terms are introduced in (1): ν is a coefficient of hyperviscosity for smooth numerical behavior and Δ denotes the horizontal Laplacian operator. α is a "Newtonian cooling" coefficient for the simplest possible representation of diabatic processes in the vorticity equation; Q is relaxed to a prescribed, zonally symmetric equilibrium state $Q_0(\phi)$ with time-scale of α^{-1}. If these damping terms are set to be zero, Q is a Lagrangian tracer which is conserved following the fluid motion.

Equation (1) is numerically integrated from an initial equilibrium state $Q = Q_0$ with a prescribed wave forcing F. A pseudospectral method with a triangular truncation of T85 is used for the computation of the advection term; grids for the spectral transformation are 256 (longitude) $\times$ 128 (latitude). The Runge-Kutta-Gill method is used for time integrations with an increment of 0.01 day. Through this study the hyperviscosity coefficient is fixed at a small constant which gives a dissipation time-scale of 0.1 day at the largest total wavenumber $N = 85$. All of the computations are done in double precision.

There are some differences between the present model and that of JM: The present model is a full spherical model and has no "wall" at the equator. The spatial resolution of T85 is not so high as their T159, although both resolutions are very high compared with traditional stratospheric models. Only the hyperviscosity was included in JM and the effect of the "Newtonian cooling" was not investigated.

Eleven series of numerical experiments listed in Table 1 are done to make a methodical sweep of parameter space. Initial configurations of $Q_0(\phi)$ used in this study are shown in Fig. 1 together with the corresponding initial zonal wind $u_0(\phi)$. The streamfunction $\psi_0(\phi)$ for the configuration I is given by a single Legendre polynomial $P_3(\sin\phi)$, while that for II by $P_2(\sin\phi)$. Latitudinal configuration of I$'$ for

Table 1. Summary of experiments. The last column denotes subsection in Section 3.

series #	Q_0	$B(\phi)$	m	α	subsection
1	I	standard	1	0	*a*
2	I	narrow	1	0	*b*
3	I	standard	2	0	*b*
4	I−	standard	1	0	*c*
5	I+	standard	1	0	*c*
6	II	standard	1	0	*d*
7	I′	standard	1	0	*d*
8	IIIa	standard	1	0	*d*
9	IIIb	standard	1	0	*d*
10	IIIc	standard	1	0	*d*
11	I	standard	1	$0.1(\text{day})^{-1}$	*e*

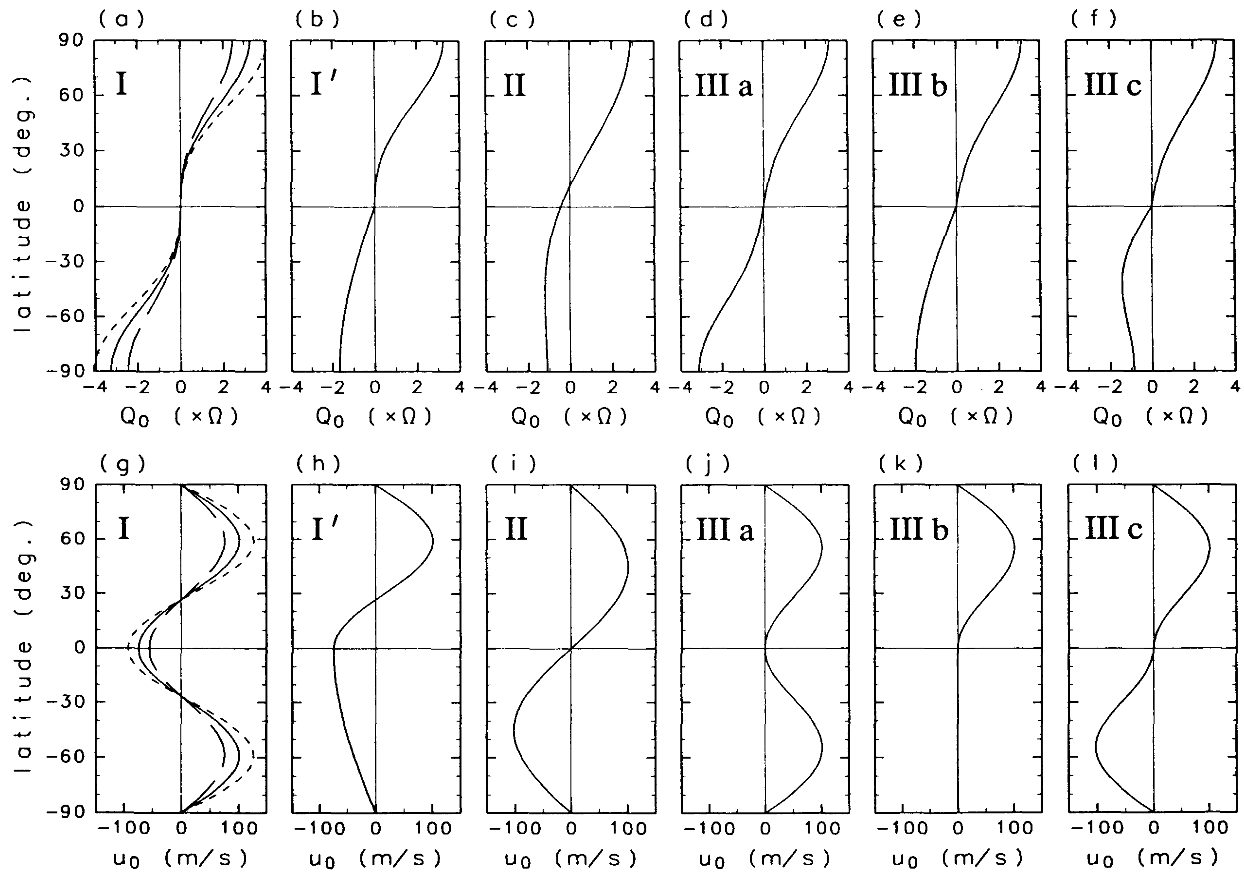

Fig. 1. Latitudinal configuration of initial absolute vorticity $Q_0(\phi)$ (top) and that of initial zonal wind $u_0(\phi)$ (bottom). Dashed lines in (a) and (g) are corresponding to the configurations I− and I+.

Series #7 is identical to I in a hemisphere ($\phi \geq 0°$) but $\psi_0(\phi \leq 0°)$ is given by $P_1(\sin\phi)$. This configuration I′ is used to investigate the sensitivity of the evolution to the initial state in the other hemisphere where the wave forcing is absent for all the integration period. Three initial configurations of IIIa, b and c for #8–#10 are also used to investigate the sensitivity to the configuration in the other hemisphere. The corresponding streamfunctions are given as follows: IIIa, $\psi_0(\phi) \propto -\sin^3\phi$; IIIb, $\psi_0(\phi) \propto -\sin^3\phi$ for $\phi \geq 0°$ and 0 for $\phi \leq 0°$; IIIc, $\psi_0(\phi) \propto -|\sin^3\phi|$. The maximum value of $u_0(\phi)$ is set to 100 m/s in each configuration.

The prescribed, time-dependent wave forcing $F(\lambda, \phi, t)$ is given by the following form (see Juckes, 1989):

$$F(\lambda, \phi, t) = 2\Omega \times F_0 A(t) B(\phi) \cos m\lambda. \tag{3}$$

The time dependence $A(t)$ shown in Fig.2(a) is assumed as

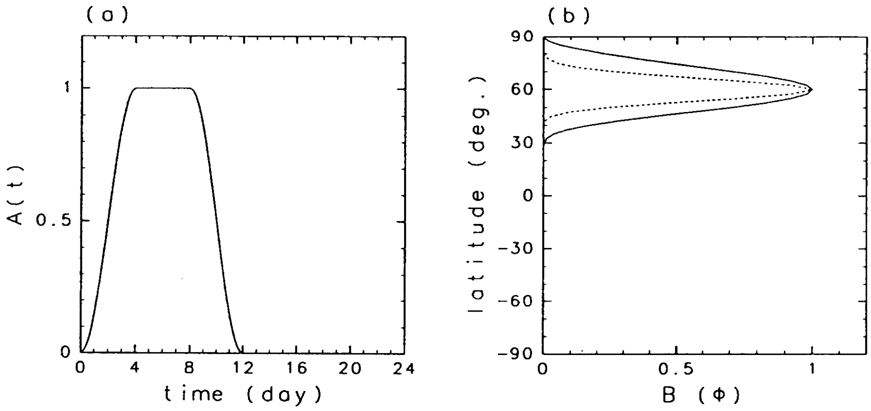

Fig. 2. Time dependence $A(t)$ of the wave forcing (a) and its latitudinal dependence $B(\phi)$ (b). Solid line in (b) is a standard width and dashed line a narrow one.

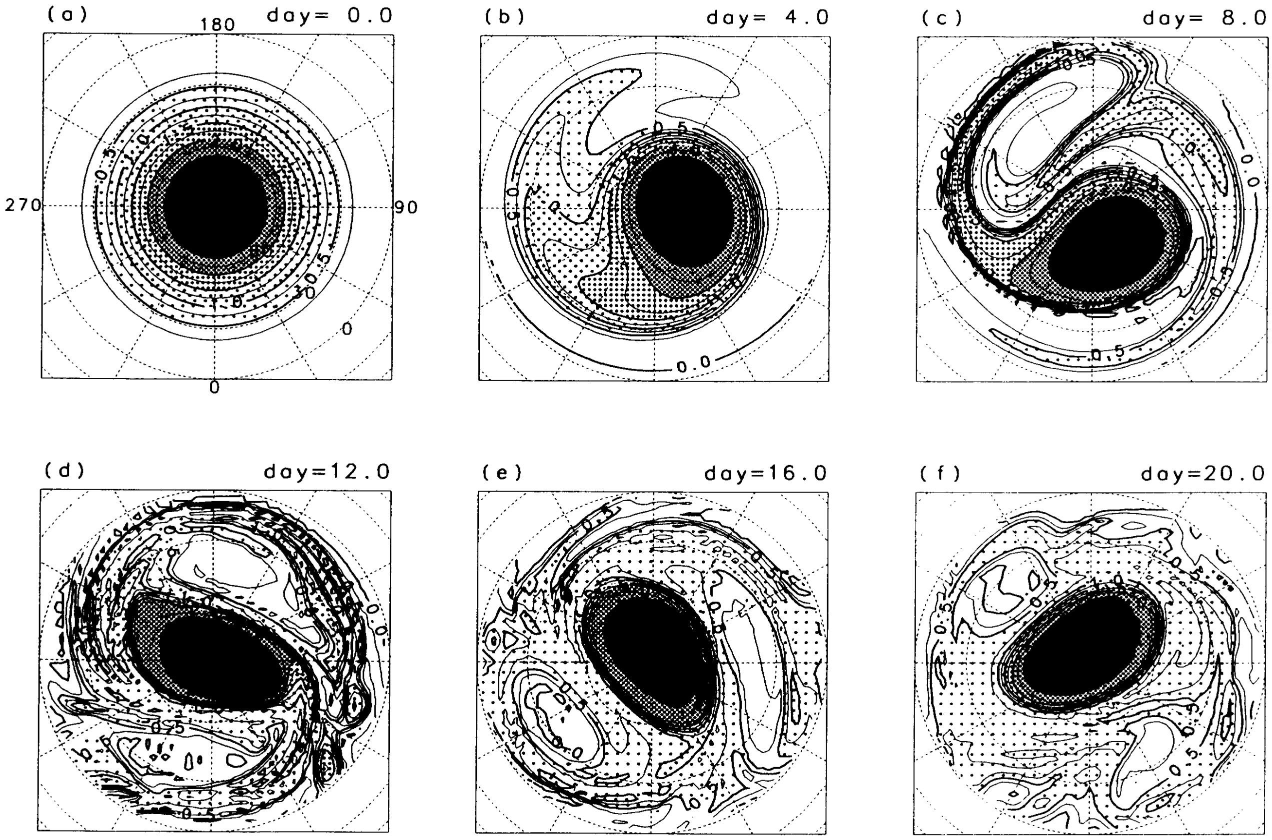

Fig. 3. Q field at the times indicated above for the control experiment of $m=1$ wave forcing when $F_0=0.3$. The contour value is scaled by Ω and dark shading corresponds to high Q. Lambert equal area projection is used only for a hemisphere ($\phi \geq 0°$). Meridians and parallels are drawn for every 30°.

$$A(t)=\begin{cases} 0.5(1-\cos(\pi t/4)), & 0\leq t\leq 4, \\ 1, & 4\leq t\leq 8, \\ 0.5(1+\cos(\pi(t-8)/4)), & 8\leq t\leq 12, \\ 0, & 12\leq t, \end{cases} \quad (4)$$

where the unit of time is day. Here $A(t)=1$ for 4 days, which is a half of the duration used by JM. The latitudinal dependence $B(\phi)$ for standard width is given by

$$B(\phi)=\begin{cases} \dfrac{\cot^2\phi}{\cot^2\phi_1}\exp\left(1-\dfrac{\cot^2\phi}{\cot^2\phi_1}\right), & \phi\geq 0°, \\ 0, & \phi\leq 0°, \end{cases} \quad (5)$$

where ϕ_1 is the latitude at which $B(\phi_1)=\max B(\phi)=1$. In this study the maximum of the wave forcing is placed at $\phi_1=60°$ as shown in Fig. 2b with a solid line. Another $B(\phi)$ with narrow width, which is drawn by a dashed line in Fig. 2b, is used in the

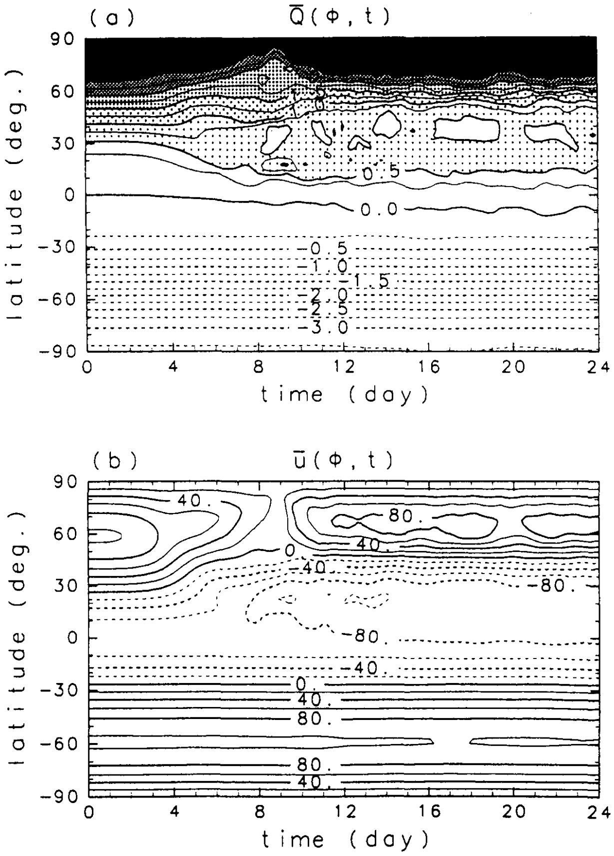

Fig. 4. Time-latitude sections of the zonal mean $\overline{Q}$ (a) and the zonal mean wind $\overline{u}$ (b) for the same run as in Fig. 3. The contour value of $\overline{Q}$ is scaled by Ω, and the contour interval for $\overline{u}$ is 20 m/s. Negative contours are drawn by dashed lines.

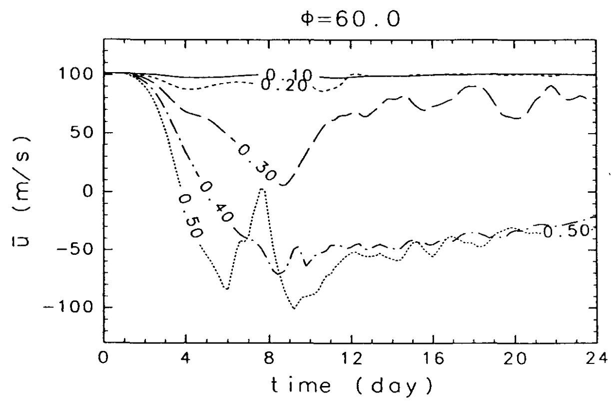

Fig. 5. Time variation of the mean zonal wind at $\phi = 60°$ for five values of F_0 from 0.1 to 0.5 in the control experiment.

Series #2; the standard $B(\phi)$ is raised to the fourth power for the narrow wave-forcing. Zonal wavenumber $m = 1$ is used for the prescribed forcing except for the Series #3. In each series of the experiments, amplitude of the wave forcing F_0 is assumed to have several values from 0.1 to 0.5 or more as the first experimental parameter.

The "Newtonian cooling" coefficient α is set to be zero in the experiments of #1–#10 to investigate the dynamic process during the vortex erosion or breakdown. A non-zero value of $\alpha = 0.1$ (day)$^{-1}$ is adopted in the last series of experiments #11 to see the relative importance of the diabatic process to the dynamic process in the recovery period of the polar vortex.

3. Results

a. Control experiment (#1)

Figure 3 shows an example of the evolution of the Q field for a control experiment similar to JM. The initial zonal wind is westerly in high and middle latitudes, while easterly in low latitudes denoted by a solid line in Fig. 1g. The amplitude of the $m = 1$ wave forcing F_0 is 0.3, which is identical to the value taken by JM, and the latitudinal configuration of the forcing is not very different from theirs as shown in Fig. 2b. The evolution resembles their result of Figs. 3–5, particularly until Day 6. A typical planetary-wave breaking process is observed: Fluid particles are well mixed outside the polar vortex and latitudinal gradients of Q are reduced there. The mixing region was named "surf zone" by McIntyre and Palmer (1983). The main polar vortex remains as an isolated material entity with sharp gradients of Q at the edge of the vortex. The sharpness of the gradients increases during the breaking process. Deformation of the polar vortex by transient planetary waves is still significant after the wave forcing was reduced to zero.

Figure 4 shows time-latitude sections of $\overline{Q}(\phi, t)$, or the zonal mean of $Q(\lambda, \phi, t)$ in (a) and the mean zonal wind $\overline{u}(\phi, t)$ in (b) for the same run as in Fig. 3. Sharp gradients of $\overline{Q}$ appear around $\phi = 60°$ after day 10, while the gradients become very gentle between 20° and 50°. These features of $\overline{Q}$ are reflection of the main vortex/surf zone structure after the wave breaking event. As for the evolution of $\overline{u}$, the westerly jet around $\phi = 60°$ decelerates largely and the latitude of maximum $\overline{u}$ shifts poleward during the initial period of the wave forcing. After the decrease of wave forcing, the westerly jet recovers at a higher latitude with a narrower width. The easterly wind in low latitudes is intensified by the wave forcing. Hints of time-variation in the other hemisphere, in which *in situ* wave forcing is absent, are also seen in both $\overline{Q}$ and $\overline{u}$, if we concentrate on some contours.

The sensitivity of the evolution of the circumpolar vortex to the amplitude of the wave forcing is investigated for several values of F_0 from 0.1 to 0.5 (Fig. 5). As a crude measure of the evolution of the vortex, the mean zonal wind $\overline{u}$ at a latitude $\phi = 60°$

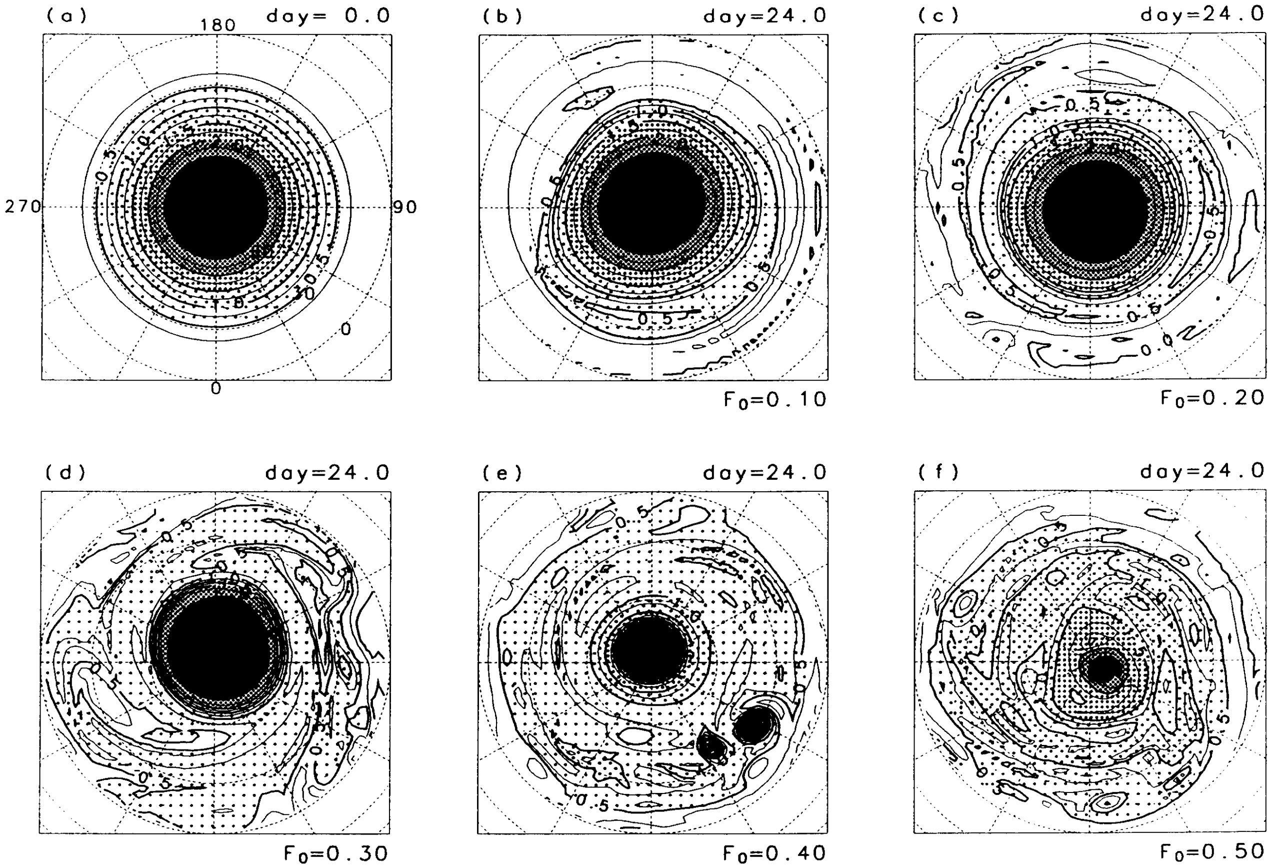

Fig. 6. Initial Q field (a) and those at Day 24 for five values of F_0 (b–f) in the control experiment.

is used in this study in addition to daily Q maps. The mean zonal wind is a primitive measure but very familiar one in the study of stratospheric sudden warmings. When the amplitude F_0 is as small as 0.1 or 0.2, the mean zonal wind $\overline{u}(\phi=60°)$ is perturbed little. When $F_0=0.3$, it decelerates until Day 9 but rapidly recovers to strong westerly wind after that time as already shown in Fig. 4b. When $F_0=0.4$ or 0.5, on the other hand, it changes to easterly wind during the forcing period and never recovers to a westerly wind.

The Q fields at day 24 for these five cases are shown in Fig. 6b–6f together with the initial field in (a). When $F_0=0.1$, 0.2 or 0.3, the high Q area of the main polar vortex is nearly conserved for the integration period. Sharp gradients of Q are formed at the edge of the vortex, which are located in lower latitudes for smaller F_0. Fluid particles outside the polar vortex are irreversibly mixed. Thus the quantity Q is not conserved in the area of the irreversible mixing, because the hyperviscosity term is not negligible there owing to strong strain fields. On the other hand, the polar vortex is largely eroded when $F_0=0.4$ or 0.5; particularly for the last case (f), most of the polar fluids are shed out and mixed well with the surroundings.

Figure 7 shows the latitudinal configurations of $\overline{Q}$ (top) and $\overline{u}$ (bottom) at Day 24 for these five cases. The latitudinal configurations support the Rossby-wave breaking process that was schematically illustrated first by McIntyre (1982, Fig. 5). The PV or Q is well mixed (*i.e.*, $\partial\overline{Q}/\partial\phi$ is small) in the breaking region, "surf zone", which locates around the critical latitude of the forced stationary Rossby waves where $u_0=0$. The mixing region becomes wider for larger F_0, and $\overline{Q}$ is largely reduced even in the polar region when $F_0=0.5$. As a result of the mixing, sharp gradients of $\overline{Q}$ appear in middle latitudes, which gradients become steep and shift poleward for large F_0. The mean zonal wind is reduced around the critical latitude owing to the breaking Rossby waves, and the westerly jet in high latitudes becomes narrow and tight, typically when $F_0=0.3$. For larger F_0 of 0.4 or 0.5, the westerly jet is largely reduced.

b. Latitudinal and longitudinal scales of the wave forcing (#2, #3)

Dependence of the Rossby-wave breaking on the latitudinal width of the wave forcing is investigated with the narrow $B(\phi)$ shown in Fig. 2b. Other conditions are identical to the control experiment #1. Figure 8a shows time variation of $\overline{u}(\phi=60°)$ for ten values of F_0 from 0.1 to 1.0. If compared with Fig. 5, it is clear that deceleration of the mean zonal

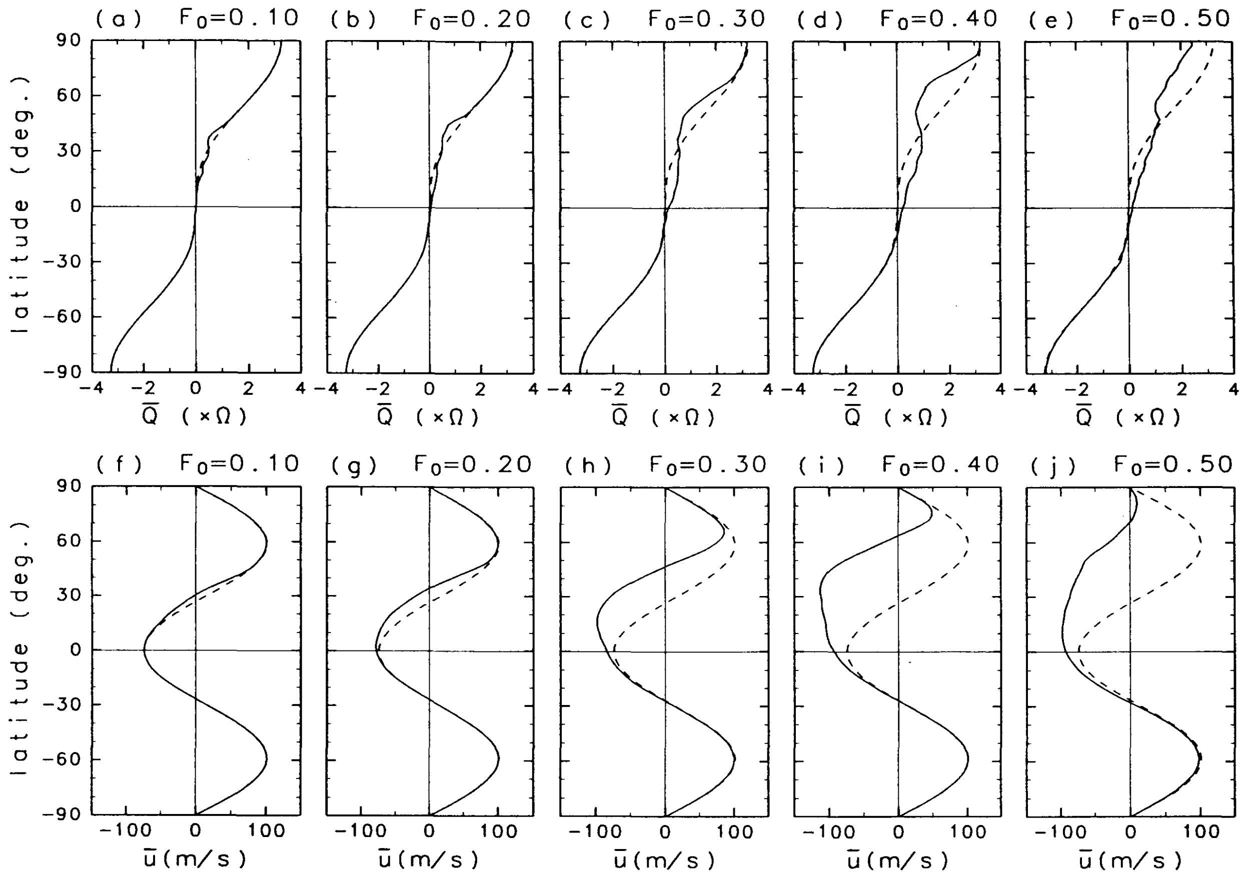

Fig. 7. Latitudinal configurations of $\overline{Q}(\phi)$ (top) and $\overline{u}(\phi)$ (bottom) at Day 24 for five values of F_0 in the control experiment. The dashed line denotes the initial configuration.

wind at $\phi = 60°$ is weakened for the narrow case. For example, the mean zonal wind nearly recovers to the initial value even if $F_0 = 0.4$ in the narrow case. Note that the intensity of the easterly wind at $\phi = 60°$ after the wave breaking is nearly the same for the amplitude F_0 from 0.6 to 1.0.

Dependence on the zonal wavenumber of the forcing is also studied for the case of $m = 2$ with the same condition as the control experiment (Fig. 8b). The wavenumber 2 forcing is more effective than that of wavenumber 1 to break the polar vortex if the amplitude of the forcing is the same. The mean zonal wind is reduced to 20 m/s when $F_0 = 0.2$ and it changes to easterly wind when $F_0 \geq 0.3$. The high Q area (not shown) is split into two areas during the forcing period even if the amplitude is small; the split of the main polar vortex promotes the mixing of Q in wide region.

c. *Intensity of the polar vortex (#4, #5)*

Dependence of the evolution on the intensity of the initial polar vortex is studied by changing the intensity ±25 % with the same $P_3(\sin\phi)$ configuration of the streamfunction (two dashed lines in Fig. 1). Figure 9 shows the time variation of the mean zonal wind at $\phi = 60°$ for the weak-vortex case I− in (a) and the strong-vortex case I+ in (b). For the weak-vortex case, the mean zonal wind recovers to westerly even if the amplitude of the wave forcing F_0 is as large as 0.5. For the strong-vortex case, on the other hand, the evolutions are classified into two groups; the mean zonal wind almost recovers to the initial value when $F_0 = 0.1$, 0.2 or 0.3, while it changes to strong easterly wind when $F_0 = 0.4$ or 0.5. The critical amplitude of the wave forcing that separates the two groups is $F_0 \sim 0.38$.

Sensitivity of the evolutions to F_0 in the three series of experiments with different intensity of Q_0 is summarized in Fig. 10, which shows $\overline{u}(\phi = 60°)$ at Day 24 for each value of F_0. The mean zonal wind changes little from the initial value when $F_0 = 0.1$ or 0.2 and decreases somewhat when $F_0 = 0.3$ in all the three cases. Drastic change in the response of the mean zonal wind takes place around $F_0 \sim 0.38$ for the strong-vortex case I+. The difference of the response between 0.3 and 0.4 decreases as the intensity of the vortex decreases.

The Q fields at Day 24 for the strong-vortex case are shown in Fig. 11. When $F_0 = 0.1$, 0.2 or 0.3, the high Q area in the polar region is not eroded very much and strong mixing takes place in low latitudes. For large wave forcing, on the other hand, the po-

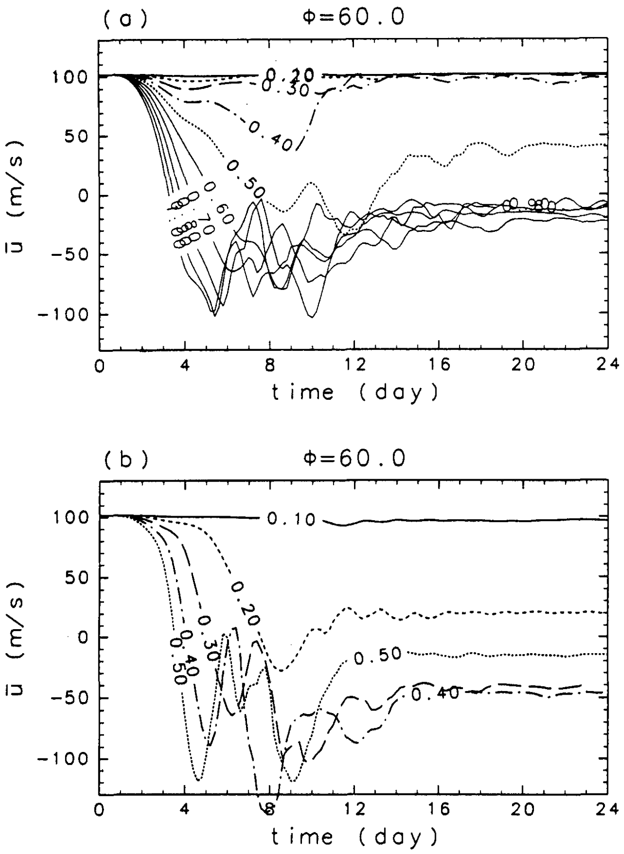

Fig. 8. Same as Fig. 5, but for the narrow wave-forcing (a) and for the $m=2$ wave-forcing (b).

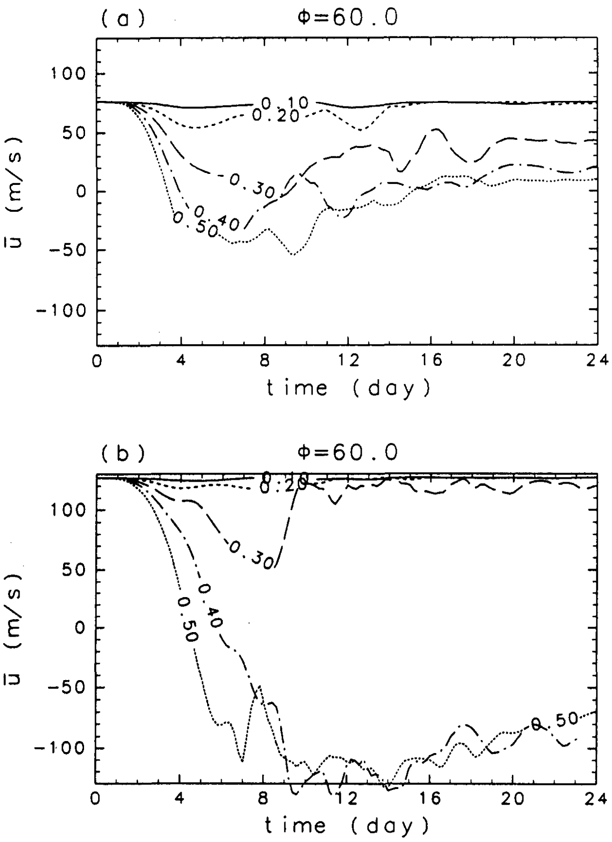

Fig. 9. Same as Fig. 5, but for the weak-vortex case with the initial zonal wind reduced to 3/4 (a) and for the strong-vortex case with the initial zonal wind increased to 5/4 (b).

lar vortex breaks into two ($F_0=0.4$) or three ($F_0=0.5$) vortices, which keep their coherent structure as an isolated material entity for all the integration period. Remember that zonal wavenumber m of the wave forcing is not 2 nor 3 but 1. Figure 12 shows the latitudinal configurations of $\overline{Q}$ and $\overline{u}$ at Day 24 for the strong-vortex case. For the large wave forcing F_0 of 0.4 and 0.5, latitudinal gradients of $\overline{Q}$ become small in a hemisphere ($\phi \geq 0°$) as a result of strong mixing, and the mean zonal wind changes to easterly over the hemisphere. The drastic change in the response between 0.3 and 0.4 is also found in Figs. 11 and 12.

Figure 13 shows an example of the evolution of coherent vortices when $F_0=0.4$. Nearly half of the polar fluid with high Q is shed out by Day 9(d), and a secondary vortex is formed (e). Two vortices keep coherent structure and are advected westward by easterly winds shown in Fig. 12i. The coherent structure survives for such a long period, because the dispersion effect of Rossby waves is very weak after the wave breaking; latitudinal gradients of $\overline{Q}$ become very small in the hemisphere as a result of strong mixing (Fig. 12d).

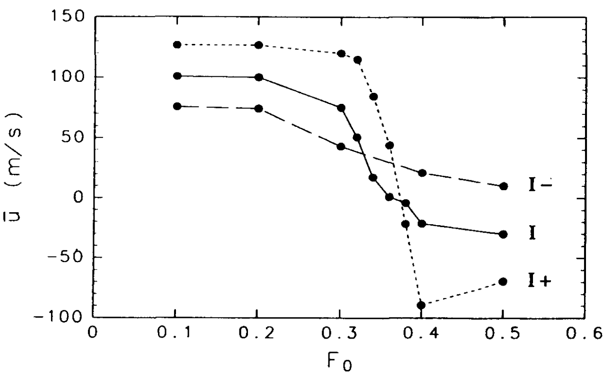

Fig. 10. Dependence of $\overline{u}(\phi=60°)$ at Day 24 on the amplitude of wave forcing F_0 for three cases of I−, I and I+.

d. Latitudinal configuration of the polar vortex (#6–# 10)

Several series of experiments were done for some different latitudinal configurations of the initial polar vortex. Figure 14a is a result for series #6 with the configuration Q_0 of II shown in Fig. 1c, the streamfunction of which consists of a single Legendre polynomial of $P_2(\sin\phi)$. The response is quite dif-

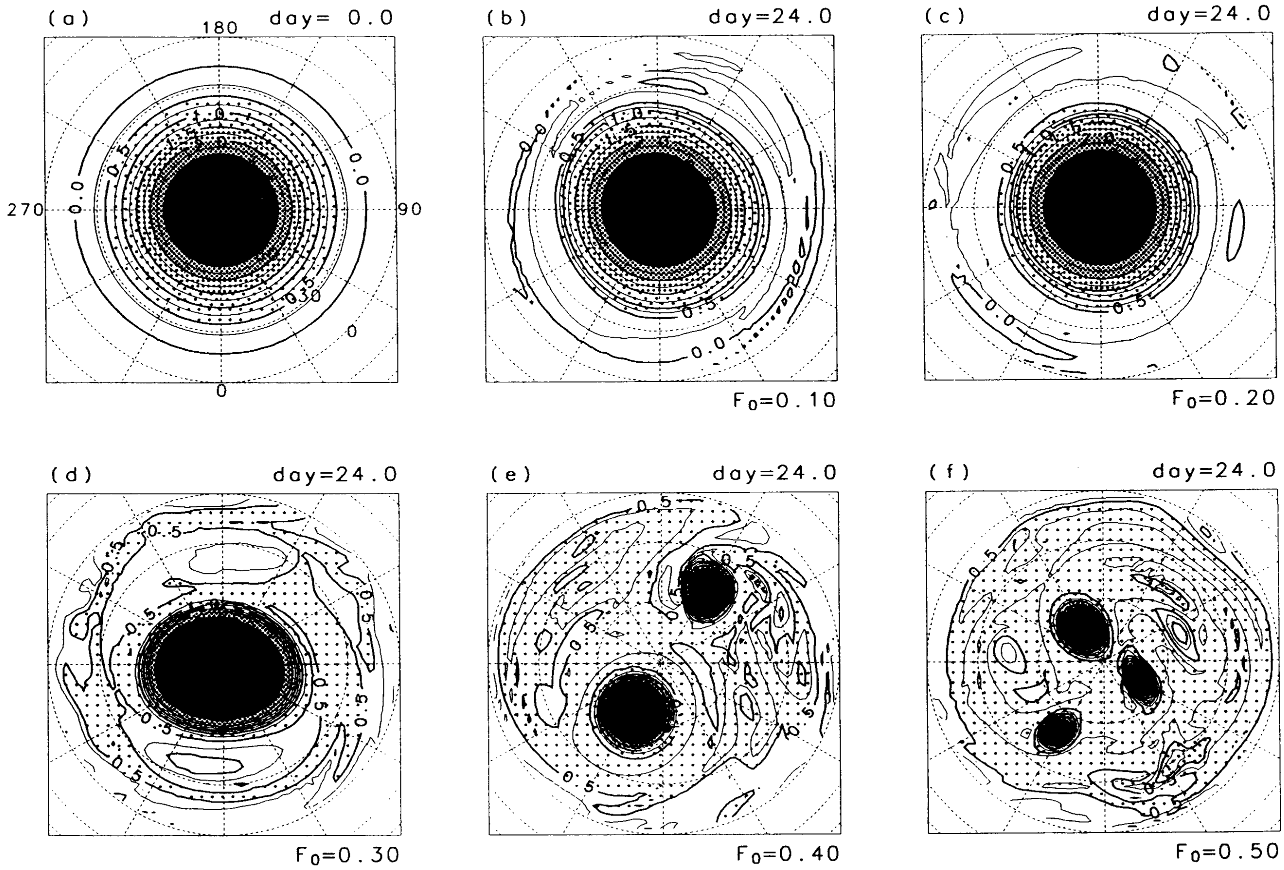

Fig. 11. Same as Fig. 6, but for the strong-vortex case. The initial value of $Q_0(\phi)$ is increased to 5/4 of the standard value of I.

ferent from that in the control experiment (Fig. 5); the mean zonal wind at $\phi = 60°$ almost recovers to the initial value for all the amplitudes F_0 from 0.1 to 0.5. The polar vortex of this initial configuration is very robust for the Rossby-wave perturbations with large amplitude.

As shown in Fig. 1i, maximum value of the initial zonal wind of the configuration II is the same as that for the configuration I but it is located at $\phi = 45°$. Critical latitude for stationary Rossby waves also shifts to the equator. Furthermore, the initial zonal wind is largely different in the hemisphere where the wave forcing is absent: It is strong westerly for Configuration I, which is symmetric with respect to the equator. On the other hand, it is strong easterly for Configuration II, which is anti-symmetric. To investigate the sensitivity to the latitudinal configuration further, another series of experiments #7 are done with the initial configuration I$'$ shown in Fig. 1b and 1h; the initial state for $\phi \geq 0°$ is identical to that for I and the difference is only in the other hemisphere. For this configuration I$'$, the mean zonal wind recovers to strong westerly even if the amplitude of the wave forcing is large (Fig. 14b). If this result is compared with the control experiment shown in Fig. 5, it is found that the response is very sensitive to the initial zonal wind in the other hemisphere particularly for the cases of large amplitude of the wave forcing ($F_0 = 0.4$ or 0.5).

Robustness of the initial zonal wind that is anti-symmetric with respect to the equator is investigated in the experiments #8–#10 with other configurations of Q_0. As shown in Fig. 1, the initial zonal wind in $\phi \geq 0°$ is the same for three Configurations IIIa, b and c. However, it is symmetric with the equator for IIIa, zero in $\phi \leq 0°$ for IIIb, and anti-symmetric for IIIc. Sensitivity of the evolution to F_0 in the three series of experiments is summarized in Fig. 15. If the initial zonal wind is anti-symmetric (IIIc), the mean zonal wind $\overline{u}(\phi = 60°)$ at Day 24 changes little from the initial value for all F_0 from 0.1 to 0.5. This is very similar to the result of series #6 with another anti-symmetric configuration of initial zonal wind. On the other hand, the response in the case of the symmetric configuration IIIa is similar to that of the control experiment shown in Fig. 10; drastic change in the response of the mean zonal wind takes place between 0.3 and 0.4. The response in the case of IIIb is intermediate of IIIa and c.

e. "Newtonian cooling" (#11)

In order to investigate recovery process of the po-

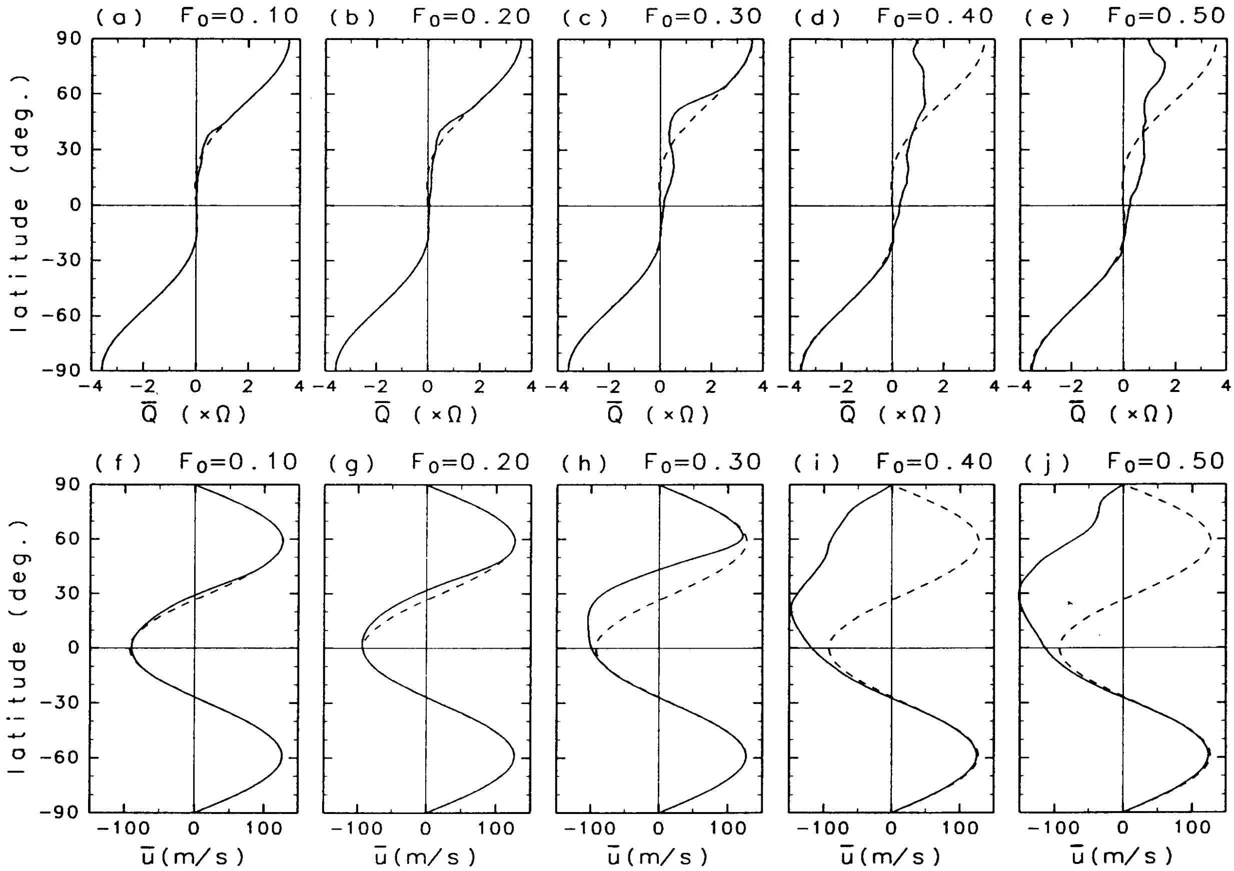

Fig. 12. Same as Fig. 7, but for the strong-vortex case. The initial value of $Q_0(\phi)$ is increased to 5/4 of the standard value of I.

lar vortex after the wave breaking events, a series of experiments were done with the "Newtonian cooling" term; the coefficient α is set to $0.1(\text{day})^{-1}$. Other experimental parameters are identical to the control experiment. Figure 16 shows evolution of the mean zonal wind at $\phi = 60°$. The time-variations until Day 4 have little difference from those in the control experiment (Fig. 5). However, the diabatic effect is evident after Day 4 particularly in the cases of large breakdown of the vortex ($F_0 = 0.4$ or 0.5); the mean zonal wind recovers nearly exponentially after ceasing of the wave forcing. Thin solid lines in the figure give exponential relaxation to the initial prescribed value due to the "Newtonian cooling" after $\overline{u}(\phi = 60°)$ has a minimum value. Note that the recovery of the mean zonal wind is much faster than the diabatic process when $F_0 = 0.3$. In this case the dynamic process of the vortex migration is important in the recovery; the main polar vortex, which have migrated off the pole owing to the wave forcing, returns to the pole without much erosion after ceasing of the wave forcing.

4. Discussion

In this study the amplitude of the wave forcing F_0 in Eq. (3) is used as the first experimental parameter. The evolution of the polar vortex is largely dependent on this parameter. However, we should point out that the "intensity" of the wave forcing depends not only the amplitude but also other parameters which determine $B(\phi)$ in Eq. (3). For example, the evolutions of $\overline{u}(\phi = 60°)$ in the control experiment (Fig. 5) resemble those in the experiment #2 in which width of the wave forcing is narrow (Fig. 8a), if each line is labeled with another appropriate measure of the intensity instead of F_0. The measure should be an integrated quantity of the wave forcing over the sphere, *i.e.*, input of angular momentum, that of kinetic energy, or something else. Note that the intensity of the wave forcing also depends on evolving flow field in the present formulation of quasi-topographic wave forcing in Eq. (1); $DF/Dt = \partial F/\partial t + \boldsymbol{u} \cdot \nabla F$, where $\boldsymbol{u}(\lambda, \phi, t)$ is the velocity field. Careful consideration on this point is necessary in analyzing the result of the experiments with different intensity of the initial vortex (#1, #4 and #5), because the intensity of the wave forcing is different in these experiments even for the same value of F_0 owing to the dependence on $\boldsymbol{u}$.

One of the most interesting results in this study is the sensitivity of the evolution to the configuration of the initial state in the other hemisphere where the

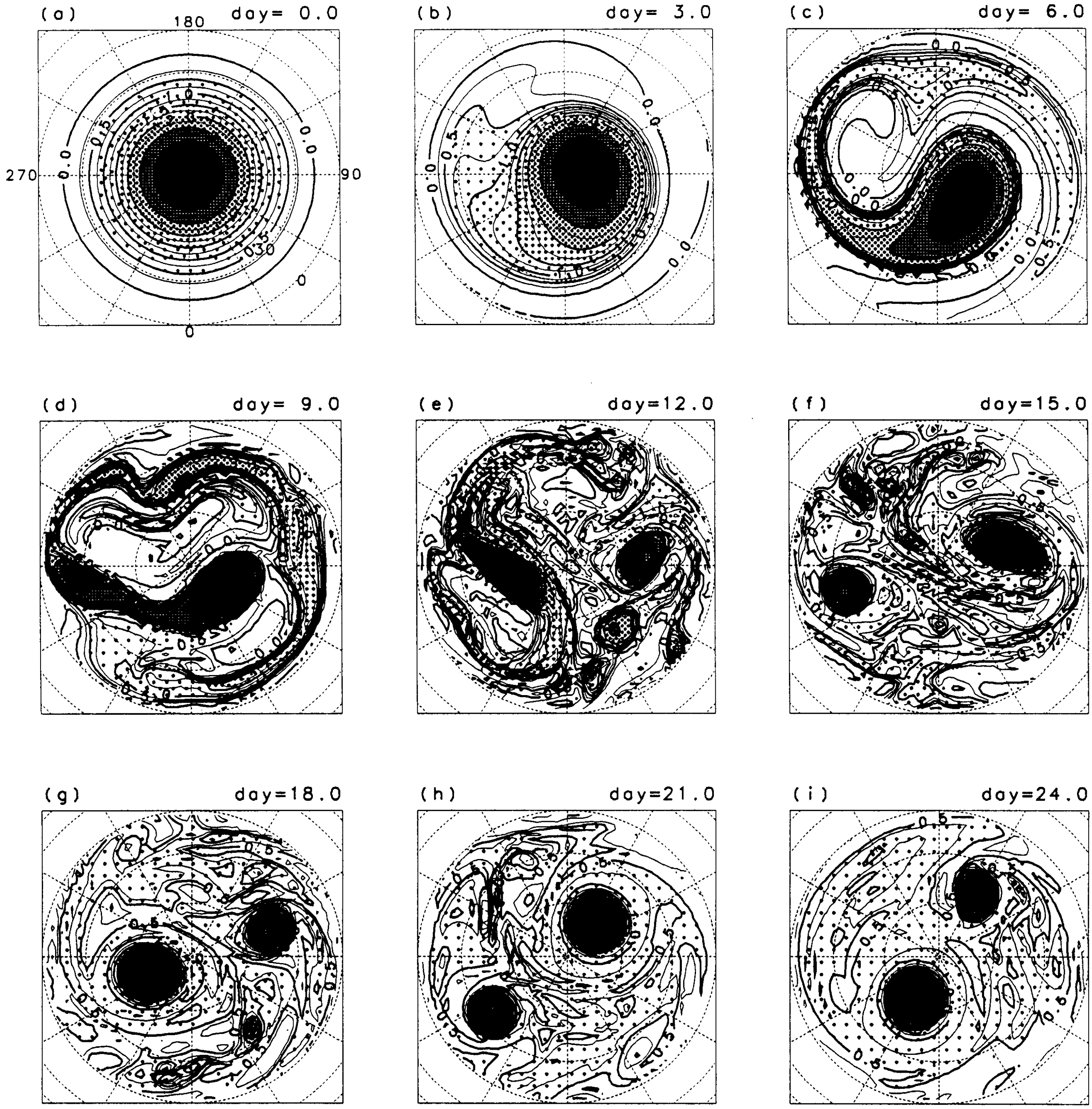

Fig. 13. Same as Fig. 3, but for the strong-vortex case when $F_0 = 0.4$. Q fields for every 3 days are shown.

wave forcing is absent. The difference between Fig. 5 and Fig. 14b and the difference in Fig. 15 are solely due to this sensitivity, because the experimental conditions are exactly the same in the hemisphere where the wave forcing exists. The sensitivity raises a question on the limitation of the theory of the non-linear critical layer when it is applied to the present experiments. The wave disturbance that is observed in the other hemisphere has a role in the evolution of the polar vortex in the experiments with initially symmetric zonal wind configuration about the equator. It is conjectured that some quantity of the forced wave survives in the low-latitude easterly winds and reflects at the other pole to influence the critical layer interaction. Data analysis of these numerical results from the viewpoint of non-linear interactions of latitudinally propagating planetary waves is an interesting subject for work in the near future.

If the mean zonal wind at a latitude $\phi = 60°$ is used to characterize the polar vortex as shown in Figs. 10 and 15, a drastic change in the response around a critical amplitude of the wave forcing is obtained in the experiments with initially symmetric zonal wind configuration with respect to the equa-

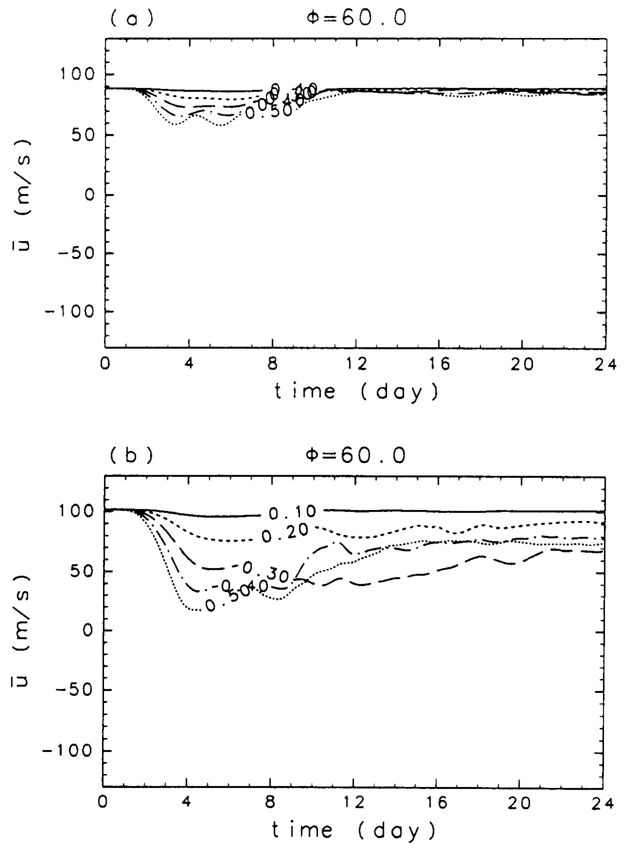

Fig. 14. Same as Fig. 5, but for the cases of latitudinal configuration Q_0 of II (a) and I′ (b).

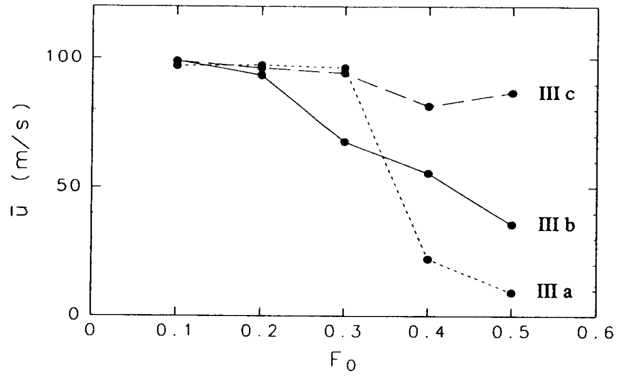

Fig. 15. Same as Fig. 10, but for three cases of latitudinal configuration Q_0 of IIIa, b and c.

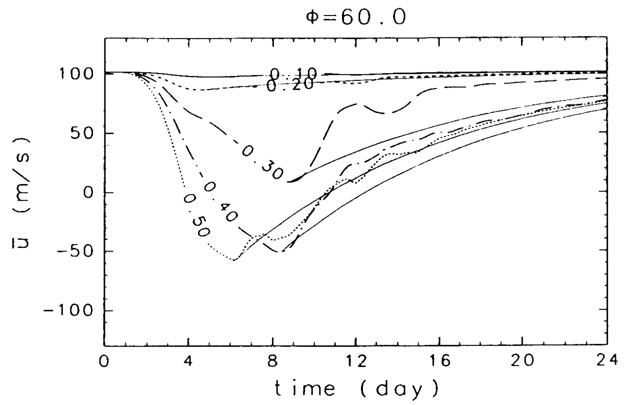

Fig. 16. Same as Fig. 5, but for the case with the "Newtonian cooling" term, $\alpha = 0.1$ $(\mathrm{day})^{-1}$. See text for thin solid lines.

tor. The drastic change is suggestive of the importance of non-linearity during the breaking process; a small change in the wave forcing around the critical amplitude brings large changes in the response. Similar suddenness of the onset of wave breaking with respect to the amplitude of wave forcing was found by Polvani and Plumb (1992) with the Contour Dynamics/Contour Surgery method, which is a different approach from conventional gridpoint or spectral models to the evolution of an isolated vortex. The suddenness in the response is an interesting correspondence between the present result and theirs, although both the models and the means of diagnosis are largely different.

Polvani and Plumb (1992) obtained some examples of secondary vortex formation for strongly supercritical amplitudes of wave forcing. A greater bulk of vortex material ejected during the breaking process rolls up into a secondary vortex. Evolution of the Q field in our results for the strong vortex case with large wave forcing, as shown in Fig. 13, has very similar configurations of the ejection and the formation of a secondary vortex. However, we have found no example of a re-merger of the secondary vortex with the main vortex, which re-merger they obtained for divergent cases with a finite value of the Rossby deformation radius. In addition to the divergent effect, the spherical geometry might be a cause of the non-existence of a re-merger in the present study, because their model is on an f-plane.

The recovery process of the polar vortex after the breakdown was investigated in the last series of Experiment #11. The result gives some insights into the reestablishment of the polar vortex after stratospheric sudden warming events. Rapid recovery of the main polar vortex due to its migration reminds us of "sudden cooling" studied by Palmer and Hsu (1983) (see also Matsuno, 1984). They described the stratospheric sudden cooling and concurrent recovery of strong westerly winds in the preconditioned period before the major sudden warming event in February 1979 with the SSU data, and pointed out the importance of non-linear wave interactions during the cooling period by a series of numerical experiments. The dynamic recovery due to the vortex migration for the case when $F_0 = 0.3$ shown in Fig. 16 is intimately related to the non-linear wave interactions they discussed, although the horizontal resolution of the present model is much higher than theirs. Moreover, the vortex re-merger obtained by Polvani and Plumb (1992) is another possible mechanism which causes the sudden cooling. It is an interesting subject to make observations on the recovery process after sudden warming events from the viewpoint obtained in this study.

The mean zonal wind at $\phi = 60°$ was used as a primitive measure of the evolution of the polar vortex. Erosion and breakdown of the main polar vortex is discussed with this measure as shown in Figs. 5, 8, 9, 14 and 16. This measure is very familiar and useful in the study of stratospheric sudden warmings, but we need a more appropriate measure with a dynamical basis to characterize the evolution of the polar vortex. For this purpose McIntyre and Palmer (1983, 1984) introduced an area index of the main polar vortex, which index was used in the analysis of the LIMS data by Butchart and Remsberg (1986). It is interesting to see the usefulness of the area index using the data obtained in the present experiments. Dynamical theory on the nonlinear evolution of a vortex (or some vortices) on a rotating sphere has not been developed satisfactorily until now compared with the development of the wave theory for a rotating sphere. It is important to establish a dynamical theory of vortex evolution.

5. Conclusions

Eleven series of numerical experiments on the evolution of a polar vortex are done with a high-resolution barotropic model in a spherical domain in order to get a deeper insight into the evolution of the stratospheric circulation during sudden warming events. A prescribed westerly circumpolar vortex is perturbed by forced Rossby waves following the pioneering work by Juckes and McIntyre (1987), and sensitivity of the evolution to several experimental parameters is investigated for wide ranges of the parameters, such as the amplitude of the wave forcing, latitudinal and longitudinal scales of the forcing, intensity of the polar vortex, and the latitudinal configuration of the vortex.

For a large amplitude of the wave forcing, the polar vortex breaks down and the absolute vorticity, which is a Lagrangian tracer after ceasing of the wave forcing, is mixed irreversibly over the hemisphere. For small amplitude of the forcing, on the other hand, the main polar vortex migrates off the pole during the forcing period and returns to the pole afterwards without much erosion. Wave forcing with wider latitudinal extent is more effective in breaking the polar vortex if the amplitude of the forcing is the same, The zonal wavenumber 2 forcing is more effective than wavenumber 1 to break the vortex. In a series of experiments with a strong initial vortex, the evolution sharply depends on the amplitude of the wave forcing; if the amplitude is below a critical value, the vortex migrates around the pole, while it breaks down if the amplitude of the wave forcing is above the critical value. Moreover, the evolution is highly dependent on the latitudinal configuration of the initial zonal wind over the globe; if the initial zonal wind is symmetric with respect to the equator, the vortex breaks easily, while it is very robust for the cases of anti-symmetric configurations of the initial zonal wind.

The recovery process of the polar vortex after ceasing of the wave forcing was also investigated in the experiments with the "Newtonian cooling" term. The relative importance of the diabatic process to the dynamic process depends on the degree of breakdown of the vortex. If the main vortex only migrates without much erosion, the dynamic process is dominant and the circumpolar vortex recovers rapidly; the time-scale is much shorter than that of diabatic relaxation. On the other hand, the polar vortex recovers slowly by the diabatic process when the vortex largely breaks down. Another dynamic process of vortex re-merger for the rapid recovery was not very effective, at least in our experiments.

Acknowledgment

GFD-DENNOU Library was used for drawing the figures.

References

Baldwin, M.P. and J.R. Holton, 1988: Climatology of the stratospheric polar vortex and planetary wave breaking. *J. Atmos. Sci.*, **45**, 1123–1142.

Butchart, N. and E.E. Remsberg, 1986: The area of the stratospheric polar vortex as a diagnostic for tracer transport on an isentropic surface. *J. Atmos. Sci.*, **43**, 1319–1339.

Clough, S.A., N.S. Grahame and A. O'Neill, 1985: Potential vorticity in the stratosphere derived using data from satellites. *Quart. J. R. Meteor. Soc.*, **111**, 335–358.

Haynes, P.H., 1990: High-resolution three-dimensional modelling of stratospheric flows: Quasi-two dimensional turbulence dominated by a single vortex. *Topological Fluid Mechanics*, Cambridge Univ. Press, 345–354.

Juckes, M., 1989: A shallow water model of the winter stratosphere. *J. Atmos. Sci.*, **46**, 2934–2955.

Juckes, M.N. and M.E. McIntyre, 1987: A high-resolution one-layer model of breaking planetary waves in the stratosphere. *Nature*, **328**, 590–596.

Kouker, W. and G. Brasseur, 1986: Transport of atmospheric tracers by planetary waves during a winter stratospheric warming event: A three-dimensional model simulation. *J. Geophys. Res.*, **91**, 13167–13185.

Leovy, C.B., C-R. Sun, M.H. Hitchman, E.E. Remsberg, J.M. Russell, III, L.L. Gordley, J.C. Gille and L.V. Lyjak, 1985: Transport of ozone in the middle stratosphere: Evidence for planetary wave breaking. *J. Atmos. Sci.*, **42**, 230–244.

Mahlman, J.D. and L.J. Umscheid, 1987: Comprehensive modeling of the middle atmosphere: The influence of horizontal resolution. *Transport Processes in the Middle Atmosphere*, D. Reidel Publishing Co., 251–266.

Matsuno, T., 1984: Dynamics of minor stratospheric warmings and "preconditioning". *Dynamics of the Middle Atmosphere*, TERRAPUB, 333–351.

McIntyre, M.E., 1982: How well do we understand the dynamics of stratospheric warmings? *J. Meteor. Soc. Japan*, **60**, 37–65.

McIntyre, M.E., 1989: On the antarctic ozone hole. *J. Atmos. Terr. Phys.*, **51**, 29–43.

McIntyre, M.E., 1990: Middle atmospheric dynamics and transport: Some current challenges to our understanding. *Dynamics, Transport and Photochemistry in the Middle Atmosphere of the Southern Hemisphere*, Kluwer, 1–18.

McIntyre, M.E. and T.N. Palmer, 1983: Breaking planetary waves in the stratosphere. *Nature*, **305**, 593–600.

McIntyre, M.E. and T.N. Palmer, 1984: The 'surf zone' in the stratosphere. *J. Atmos. Terr. Phys.*, **46**, 825–849.

O'Neill A. and V.D. Pope, 1988: Simulations of linear and nonlinear disturbances in the stratosphere. *Quart. J. R. Meteor. Soc.*, **114**, 1063–1110.

O'Sullivan, D. and M.L. Salby, 1990: Coupling of the quasi-biennial oscillation and the extratropical circulation in the stratosphere through planetary wave transport. *J. Atmos. Sci.*, **47**, 650–673.

Palmer, T.N. and C.-P.F. Hsu, 1983: Stratospheric sudden coolings and the role of nonlinear wave interactions in preconditioning the circumpolar flow. *J. Atmos. Sci.*, **40**, 909–928.

Polvani, L.M. and R.A. Plumb, 1992: Rossby wave breaking, microbreaking, filamentation, and secondary vortex formation: The dynamics of a perturbed vortex. *J. Atmos. Sci.*, **49**, 462–476.

Salby, M.L., R.R. Garcia, D. O'Sullivan and P. Callaghan, 1990: The interaction of horizontal eddy transport and thermal drive in the stratosphere. *J. Atmos. Sci.*, **47**, 1647–1665.

Salby, M.L., R.R. Garcia, D. O'Sullivan and J. Tribbia, 1990: Global transport calculations with an equivalent barotropic system. *J. Atmos. Sci.*, **47**, 188–214.

Salby, M.L., D. O'Sullivan, R.R. Garcia and P. Callaghan, 1990: Air motions accompanying the development of a planetary wave critical layer. *J. Atmos. Sci.*, **47**, 1179–1204.

Schoeberl, M.R. and D.L. Hartmann, 1991: The dynamics of the stratospheric polar vortex and its relation to springtime ozone depletions. *Science*, **251**, 46–52.

強制ロスビー波による極渦の崩壊—数値実験—

余田成男・石岡圭一

(京都大学理学部地球物理学教室)

突然昇温現象にともなう成層圏循環の変動をより深く理解するために、強制ロスビー波によって攪乱された極渦の時間発展に関する数値実験を行った。高分解能順圧全球モデルを用いて、幅広い実験パラメータ領域で時間発展のパラメータ依存性を調べた。

強制波の振幅が大きい場合には、極渦は崩壊し、力学的トレーサーである絶対渦度は半球全体にわたって不可逆的に混合される。一方、振幅が小さい場合には、極渦は強制波が加えられた期間には極から離れるが、混合によって大きく浸食されることはなく、強制がなくなると元の位置に戻る。このような極渦応答の強制波振幅に対する敏感性は、また、他の実験パラメータ (強制波の空間規模、極渦の強さ、極渦の南北構造) にも依存している。極渦は、強制波の南北の広がりが大きいほど壊れやすく、東西波数 1 よりも 2 の強制波に対して壊れやすい。また、強い極渦の場合には、ある臨界振幅を境にして極渦の応答が彷徨型から崩壊型へと突然に変化する。さらに、このような応答は、初期に与える極渦の南北構造に大きく依存している。初期東西流が赤道対称の構造であれば極渦は壊れやすく、赤道反対称であれば壊れにくい。